# NJC

Accepted Manuscript


This is an *Accepted Manuscript*, which has been through the Royal Society of Chemistry peer review process and has been accepted for publication.

*Accepted Manuscripts* are published online shortly after acceptance, before technical editing, formatting and proof reading. Using this free service, authors can make their results available to the community, in citable form, before we publish the edited article. We will replace this *Accepted Manuscript* with the edited and formatted *Advance Article* as soon as it is available.

You can find more information about *Accepted Manuscripts* in the Information for Authors.

Please note that technical editing may introduce minor changes to the text and/or graphics, which may alter content. The journal's standard Terms & Conditions and the Ethical guidelines still apply. In no event shall the Royal Society of Chemistry be held responsible for any errors or omissions in this *Accepted Manuscript* or any consequences arising from the use of any information it contains.

ROYAL SOCIETY OF CHEMISTRY

www.rsc.org/njc

NJC

ARTICLE

# Monolithic magnetic carbonaceous beads for efficient Cr(VI) removal from water

Received 00th January 20xx,
Accepted 00th January 20xx

DOI: 10.1039/x0xx00000x

www.rsc.org/

Zhi-Min Lei,[a] Qing-Da An*,[a] Yuan Fan,[a] Jia-Liang Lv,[a] Ce Gao,[a] Shang-Ru Zhai*,[a] Zuo-Yi Xiao[a]

Monolithic, magnetic carbonaceous materials as adsorbents can provide easy recovery and quickly separate pollutants in wastewater treatment; however, the developing of designed fabrication process remains a great challenge. Herein, a super magnetic monolithic material was firstly synthesized *via* a controllable carbonization of ferric alginate beads; and its adsorption behaviours of Cr(VI) were investigated in detail. This new adsorbent was characterized using field emission scanning electron microscopy (FESEM), energy dispersive spectrometer (EDS), transmission electron microscopy (TEM), $N_2$ adsorption-desorption isotherms, X-ray diffraction (XRD), Raman spectrum, vibrating sample magnetometer (VSM), Zeta-potential, Fourier transform infrared spectroscopy (FTIR) and X-ray photoelectron spectroscopy (XPS). Kinetic and equilibrium studies indicated that the experimental data of Cr(VI) adsorption were better described by pseudo-second-order kinetic and Langmuir models. The maximum adsorption capacity of the material for Cr(VI) was calculated to be 143.20 mg $g^{-1}$ at room temperature. Evaluation of the thermodynamics parameters ($\Delta H > 0$, $\Delta S > 0$, and $\Delta G < 0$) revealed the adsorption process was endothermic and spontaneous. The mechanism study showed that the adsorption of Cr(VI) likely involved electrostatic attraction and redox reaction. It was demonstrated that the material was an effective adsorbent for Cr(VI) removal with quick separation; most importantly, compared to those conventional powdery adsorbents, this bead-like material could be handled much more conveniently for re-usage and scale-up for the practical application owing to its easily operability and separation.

## Introduction

The increasing contamination of urban and industrial wastewater by toxic metal ions causes serious environmental problem.[1] Chromium is a common contaminant in surface water and groundwater due to its widespread use in industrial activities such as: leather tanning, electroplating, manufacturing of dye and paint, pulping and papermaking, and the petroleum refining. The Cr(VI) is highly toxic, carcinogenic and mutagenic to the environment and all forms of living organisms.[2,3] Owing to its high toxicity and mobility in the aqueous media, it has become a global challenge to remove Cr(VI) from wastewater in a highly efficient manner.[4] A maximum allowable limit of 0.05 mg $L^{-1}$ for total chromium has been set by the World Health Organization (WHO) drinking water guidelines, and the permissible Cr(VI) concentration in drinking water is 0.05 mg $L^{-1}$ in China.[5] Therefore, it is necessary to reduce Cr(VI) concentration to an acceptable level in both potable water and industrial wastewater discharges for environmental protection.

Various techniques have been developed to eliminate Cr(VI) from wastewater including chemical precipitation,[6] ion exchange,[7] membrane filtration,[8] solvent extraction,[9] adsorption[10] and biological process,[11] etc. However, each of the techniques has certain drawbacks. Chemical precipitation generates a toxic sluge; there is a high cost associated with using ion-exchange resins; and the efficiency achieved by membrane treatments is often quite low. In contrast, adsorption has attracted much attention due to its significant advantages such as simplicity of design and operation, cost-effective, high efficiency, recycle of adsorbent and no secondary pollution caused by the by-products.[12]

In the past years, activated carbon has been widely used as contaminant removal media to tackle Cr(VI) in water pollution problems considering its simplicity, cheap, easy to scale-up and ability to remove low concentration contaminants.[13] The adsorption of heavy metals by activated carbon greatly relies upon its physical properties such as specific surface area and pore size distribution and surface chemistry. However, the cost of generation and regeneration of activated carbon is relative expensive. Due to this difficult problem, the production of low cost and reusable sorbents for removal Cr(VI) is worth considering.

Magnetic materials have been introduced into the adsorbent recently, and the magnetic separation method has been considered as high separation efficiency, low cost and convenient technique in comparison with the traditional separation methods such as precipitation, centrifugation or filtration.[14,45] The embedding of magnetic property into carbonaceous materials can be acquired the practical adsorbent for the tackle of Cr(VI). Despite many powdery magnetic carbonaceous materials have been developed, and achieved high efficiency. For example, Ruan *et al.*[15] have reported a method for the fabrication of rosin-based biochar coated bentonite for supporting $Fe_2O_3$ and its maximum adsorption capacity can be reached 81.7 mg $g^{-1}$. Also, Zhang and co-workers[16] have prepared chitosan-modified magnetic biochars for the removal Cr(VI), the maximum adsorption capacity can be achieved 120 mg $g^{-1}$. However, the recovery of nanometer-sized materials still exist a few

[a] Faculty of Light Industry and Chemical Engineering, Dalian Polytechnic University, Dalian 116034, China. Email: anqingda@dlpu.edu.cn; zhaisr@dlpu.edu.cn

Electronic Supplementary Information (ESI) available: SEM images, EDS spectra, $N_2$ adsorption-desorption isotherms, XRD, Raman, Zeta potential and FTIR of MMCB before and after adsorption, physical textural properties, and adsorption thermodynamic parameters. See DOI: 10.1039/x0xx00000x

disadvantages, such as, it is inherently difficult to operate and the partial loss of magnetic property on the adsorbents would bring trouble in recovering. Unlike to these powdery carbonaceous materials, the monolithic materials became a new focus point because of its monolithic characteristics and easy operability. However, it is still a challenge to fabricate monolithic materials with controllable morphology and easy handling properties for application. As is known, the monolithic materials is of macroscopic leveled substance, which can be handled much more conveniently for re-usage and practical application owing to its easily operation. Therefore, the fabrication of monolithic adsorbent is of much more interest, to meet the actual requirement as compared to the powdery adsorptive materials.

Alginate, isolated from marine algae is a copolymer of β-D-mannuronic acid (M) and α-L-guluronic acid (G).[17,46] Alginate beads could be prepared by dispersing sodium alginate into a water solution containing $CaCl_2$.[18,19,20] Calcium cation induce interchain association between long stretches of G units and the formation of the gel junction zones, and the structure has been described by the so-called egg-box model.[21,22] Consequently, the cross-linked cations can be achieved highly dispersed in the network of sodium alginate. Likewise, sodium alginate can also be cross-linked by $Fe^{3+}$ ions; nevertheless, the formed ferric alginate beads would be damaged for its poor mechanical stability. Based on our previous research, and following on continuous interest in designing functional sorbents for emerging pollutants.[23-29] Herein, an ion exchange mechanism between $Ca^{2+}$ and $Fe^{3+}$ was firstly introduced to the fabrication of hydrogel beads and after being subjected to controllable carbonization procedure, the monolithic magnetic carbonaceous beads (MMCB) was successfully prepared for the removal Cr(VI) from the aqueous system. The prepared material was characterized by various techniques. Besides, the relevant parameters such as pH, kinetics, adsorption isotherms, thermodynamic and the effect of co-existing ions were investigated in detail to study the adsorption performance of MMCB for Cr(VI) in aqueous solution; and the conceivable adsorption mechanism was also discussed.

## Materials and methods

### Chemicals

Sodium alginate, $CaCl_2$ and $FeCl_3 \cdot 6H_2O$ were purchased from Sinopharm Chemical Reagent Corporation, China. $K_2Cr_2O_7$, Ethanol, HCl and NaOH were purchased from Tianjin Kermel Chemical Reagent Factory, China. All of the Reagents were of analytical grade and were used as received without any further purification. Double distilled water was used throughout this study. Various Cr(VI) solutions with different concentration were prepared by dissolving $K_2Cr_2O_7$ in distilled water.

### Preparation of Fe-SA beads

Sodium alginate (4.0 g) was dissolved in 200 mL deionized water and stirred until evenly dispersed. The calcium alginate (CA) hydrogel beads with a mean diameter of 4 mm were obtained by drop-by-drop addition of prepared sodium alginate (2%, w/v) into $CaCl_2$ (5%,w/v) aqueous solution under continual magnetic stirring. The obtained beads were immersed in the $CaCl_2$ solution for another 6 h for complete gelling. The hydrogel beads were filtered and washed with deionized water to remove extra $Cl^-$ and $Ca^{2+}$. Subsequently, the CA beads were added into the solution containing $FeCl_3$ (3%, w/v) and kept continual magnetic stirring over night for the progress of ion exchange between $Fe^{3+}$ and $Ca^{2+}$. Afterward, the color of hydrogel beads changed from white to yellow. The obtained yellow beads were washed with distilled water and ethanol till the supernatant became colorless, and then dried in 60°C oven for 12 h. In the process of washing Fe-SA beads, the supernant became colorless and the beads color varied yellowish gradually. This pheonmenon indicated that the excess $Fe^{3+}$ which existed in the polymer chains through the weak interaction was removed, and the retained $Fe^{3+}$ was linked with carboxyl groups in the sodium alginate. This process guaranteed the highly dispersity of magnetic nanoparticles in the carbon network and can be acquired enough magnetism for the fast separation.

### Preparation of the MMCB

The dried Fe-SA beads were pyrolyzed in a tube furnace at 600°C in $N_2$ environment for 2 h. The resulted material from Fe-SA was permitted to cool at room temperature under a flow of nitrogen gas, which was referred as MMCB. Then, it was washed with 1 M HCl solution half an hour for the removal of impurities, then washed with distilled water till the supernatant was neutral and dried in an oven at 60°C. At last, they were sealed to preserve before use. The preparation process of MMCB was shown in Scheme 1.

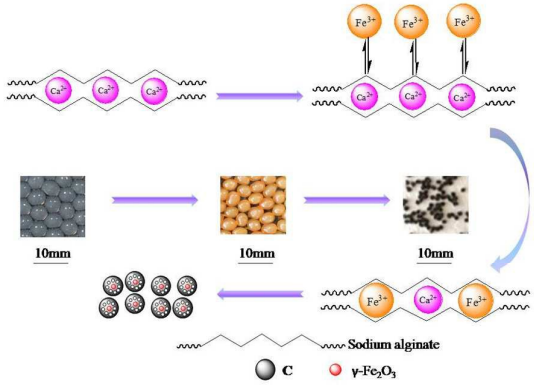


Scheme 1 Schematic illustration of the fabrication process of MMCB.

### Materials characterization

X-ray diffraction (XRD) patterns were obtained with a Shimadzu XRD-6100 diffractometer with Cu-$K_\alpha$ radiation (λ = 1.540 Å) from 10 to 80 ° at 8 ° $min^{-1}$ scanning speed. The surface morphologies and the particle distribution of MMCB were determined by field emission scanning electron microscopy (FESEM, JSM-6460LV, JEOL, Japan) and transmission electron microcopy (TEM, JEM-2000EX electron microscope, JEOL, Japan), respectively. Fourier transform infrared (FTIR, Perkin-Elmer, USA) spectra in the 4000–400 $cm^{-1}$ region were acquired by using KBr pellets. X-ray photoelectron spectroscopy (XPS) measurements were performed using the Thermo Scientific ESCALAB250 spectrometer (Thermo VG, USA) equipped with an Al-Ka X-ray source (1486.6 eV). The specific surface area and pore diameter of the samples were performed by nitrogen adsorption-desorption experiments at 77 K (Quantachrome Autosorb NOVA2200e, USA). Magnetism was analyzed by Lake Shore 7410 vibrating sample magnetometer (VSM) at room temperature. UV-Vis adsorption spectra were recorded on a MAPADA UV-1600PC spectrometer. Raman spectrometry (RM2000, Renishaw, UK) was used to study the integrity of sample. Zeta-potential analysis of the 1 wt% sample dispersed in water was measured by using Malvern Zetasizer Nano instrument at 25°C.

**Adsorption experiments**

The adsorption of Cr(VI) from aqueous system onto MMCB was studied in a batch system. In each adsorption experiment, 20 mL of Cr(VI) solution with desired concentration was put into a 50 mL conical flask. The solution pH measured by a pH meter was adjusted to a predetermined value with 0.1 M HCl or 0.1 M NaOH, and 20 mg MMCB was added into the above solution. Subsequently, the mixture was stirred in magnetic shaker to reach equilibrium except kinetic experiments. It should be noted that the MMCB would not be attracted on the magneton since their relative small magnetism; this ensured the homogeneity of system in the adsorption process. At the end of each experiment, the supernatant can be acquired directly through putting an external magnetic field under the conical flask. The residual Cr(VI) concentration in supernatant was determined with 1,5-diphenycarbohydrazide spectrophometric method using an ultraviolet spectrophotometer.

The removal efficiency ($R$ %) and the adsorption capacity of Cr(VI) at time t ($q_t$, mg $g^{-1}$) were calculated according to the formula:

$$R\% = \frac{C_0 - C_t}{C_0} \times 100\%$$

$$q_t = \frac{(C_0 - C_t) \times V}{m}$$

where $C_0$ (mg $L^{-1}$) and $C_t$ (mg $L^{-1}$) are the liquid phase concentration of Cr(VI) at initial and time $t$ (min), respectively. $V$ (L) is the volume of Cr(VI) solution, $m$ (g) is the mass of the adsorbent.

## Results and Discussion

**Characterization of MMCB**

Characterization of fresh MMCB and the one after adsorption (i.e. MMCB-Cr) is helpful to understand the properties that may affect the removal of Cr(VI) and further to interpret the removal mechanism. Surface morphology of MMCB and MMCB-Cr was studied using field emission scanning electron microscopy, which has been a primary tool for characterizing the surface morphology and fundamental physical properties of the adsorbent surface, was useful for determining the particle shape, porosity and appropriate size distribution of the adsorbent.[30] The FESEM images of the MMCB and MMCB-Cr were depicted in Fig. S1, it was clear that the surface of the sample was consisted of many nanometer particles, which was favorable to the formation of large surface area and can be supported by the following BET analysis. The inset digital photographs were the actually used adsorbent beads enlarged 100 times under the FESEM. From the photos, it was observed that the surface of the beads possessed large amounts of gaps, which emerged by the carbonization of ferric alginate beads and the ferric may help to generate the pores in the gaps.[31] The pore structure would provide enough surface and benefited the combination of the adsorption sites and Cr(VI) ions. With comparison of MMCB and MMCB-Cr, it was found that no obvious changes of the beads surface after adsorption of Cr(VI); this demonstrated that the surface of the adsorbent was not damaged by highly oxidizing Cr(VI) and possibly it can be easily regenerated by means of desorption. Also, the EDS spectra was used to identify the existence of Cr(VI) on the MMCB. As depicted in Fig. S2, it is clearly shown that the existence of Cr(VI). After adsorption of Cr(VI), the content of oxygen also increased dramatically, this can be ascribed to the oxygen of $HCrO_4^-$, further certifying the existence of Cr(VI) on the MMCB.[32]

The morphology and microstructure of MMCB and MMCB-Cr were also investigated by transmission electron microscopy (TEM). From the Fig. 1, a large number of nanoparticles were noticed on the skeleton of carbon foam, and the size of nanoparticles was of about 10 nm, suggestive of a relatively uniform dispersion in the carbon matrix.[33] The high degree of distribution of magnetic particles is owing to the electrostatic attraction between $Fe^{3+}$ and –COOH in the sodium alginate.[20] The loading of magnetic particles on the foam bring benefits to increase the surface area of foam as well as render the latter with magnetic property.

$N_2$ adsorption-desorption isotherms and pore size distribution curves of the MMCB and MMCB-Cr were illustrated in Fig. S3 and the detailed parameters were summarized in Table S1. The surface areas of MMCB and MMCB-Cr were 344.89 and 216.07 $m^2$ $g^{-1}$, respectively, which indicated that the chromium ions occupied certain pores after adsorpting Cr(VI). Additionally, the total volume of MMCB-Cr also decreased, which further proofed the existence of chromium ions on the surface of pores. The pore size is about 3.63 nm, indicative of the mesoporosity of MMCB,[34] and the high porosity of it was advantageous for mass transfer between the chromium ions and adsorption sites, which prompted the Cr(VI) adsorption capacity.

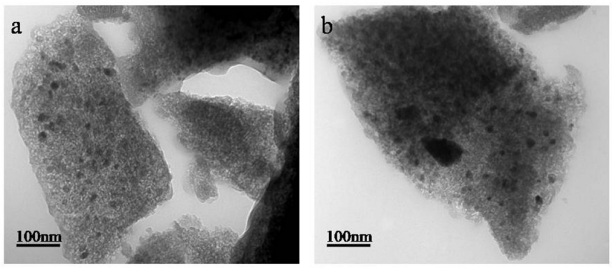


Fig. 1 The TEM images of MMCB (a) and MMCB-Cr (b).

The crystalline structures of the MMCB and MMCB-Cr were characterized by powder X-ray diffraction (XRD). As seen in Fig. S4, the peaks at 2 theta = 26° in MMCB and MMCB-Cr can be attributed to the diffraction of the (002) plane of the graphite structure,[34] which is due to carbonization under high temperature, resulting in carbon structures with some degree of graphitic order. Additionally, the peaks located at 43° and 62.7° could be ascribed to the γ-$Fe_2O_3$, according to the JCPD 39-0238.[34] It was clear that the crystalline structures of the MMCB-Cr had not changed obviously and this indicated that the structure of MMCB kept integrity after adsorption of Cr(VI).

The Raman spectrum of MMCB was presented in Fig. S5. As can be seen, the sample showed a D peak at 1343 $cm^{-1}$ and 1570 $cm^{-1}$ for G band, respectively, suggestive of the structure of $sp^3$ and $sp^2$ hybridized carbon atoms. The degree of the graphitization of MMCB can be quantified by the intensity ratio of D to G bands. The peak intensity ratio ($I_D/I_G$) was 0.45 and it implied that the carbon atoms of MMCB were amorphous in nature.

Furthermore, the MMCB possesses magnetic recovery from the aqueous phase. In Fig. 2, the hysteresis loop of MMCB at room temperature showed the typical paramagnetism characteristics. The saturated magnetization of MMCB was 0.731emu/g, which was sufficiently enough to be separated from aqueous solution by the aid of its monolithic characteristic and could not be attached on the magnet under the magnetic stirring condition. Complementary, the digital photographs (Fig. 2 inset) demonstrated that the MMCB could be readily separated after adsorption by an external magnetic

field.[35] Most importantly, the monolithic characteristic guarantee the integrity of magnetic property in the maximum extent during the adsorption process, and even hand picking from the aqueous system is possible.

**Effect of pH on Cr(VI) adsorption**

Solution pH plays an important role in Cr(VI) adsorption owing to its effect not only on the degree of speciation and ionization of Cr(VI) but also on surface charge of the adsorbent.[36] The results of Cr(VI) adsorption by MMCB with the initial solution pH ranging from 2.0 to 9.0 at initial Cr(VI) concentration of 25 mg/L as shown in Fig. 3. Clearly, the amount of Cr(VI) adsorbed on MMCB was highly pH dependent , and the $q_e$ value decreased gradually from 24.23 to 8.29 mg/g with increasing solution pH from 2.0 to 9.0, and the adsorption capacity reached the maximum value at pH 2.0. As is reported, Cr(VI) existed in different forms in aqueous solution at different pH values, such as $H_2Cr_2O_4$ (aq), $Cr_2O_7^{2-}$, $HCrO_4^-$, $CrO_4^{2-}$. $HCrO_4^-$ is the predominant Cr(VI) species at pH < 6.51, while $CrO_4^{2-}$ was predominant at pH > 6.51.[37] The adsorption free energy of $HCrO_4^-$ (-2.5 to -0.6 kcal $mol^{-1}$) was higher than that of $CrO_4^{2-}$ (-2.1 to -0.3 kcal $mol^{-1}$), thus $HCrO_4^-$ was more favourable for adsorption

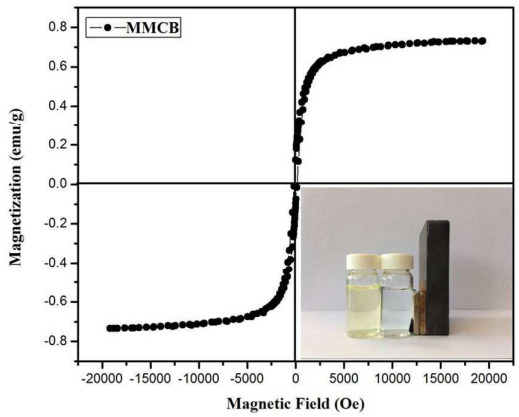


Fig. 2 The magnetic curve of MMCB and the right inset is the comparison of before and after adsorption.

than $CrO_4^{2-}$.[38] Besides, with increasing the solution pH, the concentration of $OH^-$ would have increased gradually; the competition of $OH^-$ ions for adsorption sites with Cr(VI) would occurred, resulting in a decrease in Cr(VI) uptake. Accordingly, the pH value at 2 would be an ideal parameter to further study the adsorption process over this new monolithic magnetic carbonaceous material. In addition, the reason of equilibrium pH was lower than initial pH after adsorption can be explained in the afterward adsorption mechanism discussion. To further investigate the interaction between MMCB and Cr(VI) ions, the zeta potential of MMCB at pH 7 was depicted in Fig. S6, showing a positive charge about 22.9 mV. Since the Cr(VI) existed as anions, the electrostatic attraction would facilitated the Cr(VI) removal from aqueous system.

**Adsorption kinetics**

For a possible application as an adsorbent, not only the pH influence but also the kinetics of adsorption reaction is important. Effect of initial concentration on Cr(VI) adsorption using MMCB was investigated by carrying out the experiments at different initial concentration (25, 50, 100 mg/L) and varying the contact time. With increasing concentration from 25 to 100 mg/L, the equilibrium time increased from 100 to 500 min. As depicted in Fig. 4, the adsorption rate was very high at the initial stage, due to the availability of abundant adsorption sites on the surface of MMCB and the large concentration gradient between the fluid films around the adsorbent particle. After a period of time, the remaining vacant sites were difficult to be occupied for the repulsive forces between the Cr(VI) ions on the solid and bulk phases, resulting in a low adsorption rate until reached equilibrium. The uptake amount of Cr(VI) at equilibrium was observed to increase dramatically from 24.9 to 88.9 mg/g with initial Cr(VI) concentration increased from 25 to 100 mg/L. High initial Cr(VI) concentration expanded the effective contact area with adsorbent and provided essential driving force to overcome the resistance to the mass transfer of Cr(VI) on interface.

Accordingly, the adsorption kinetics was modeled by the pseudo-first-order, and the pseudo-second-order, rate equation expressed as follows:

$$\log(q_e - q_t) = \log q_e - \frac{k_1}{2.303}t$$

$$\frac{t}{q_t} = \frac{1}{k_2 q_e^{\ 2}} + \frac{1}{q_e}t$$

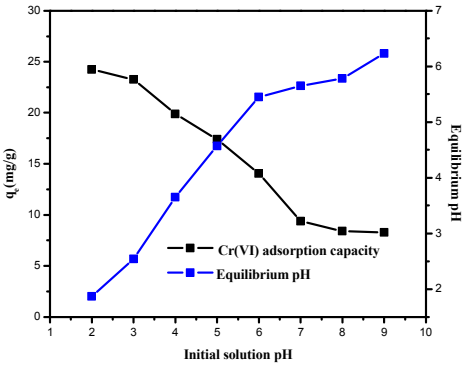


Fig. 3 Effect of initial pH on Cr(VI) adsorption and equilibrium pH

Table 1 Comparison of rate constants calculated based on respective pseudo-first-order, pseudo-second-order, and intraparticle diffusion kinetic models

| | | Pseudo-first-order | | | Pseudo-second-order | | | Intraparticle diffusion | | | | | |
|---|---|---|---|---|---|---|---|---|---|---|---|---|---|
| $C_o$ | $q_{e,exp}$ | $k_1$ | $q_{e,cal}$ | $R^2$ | $k_2$ | $q_{e,cal}$ | $R^2$ | $k_{i,1}$ | $R_1^2$ | $k_{i,2}$ | $R_2^2$ | $k_{i,3}$ | $R_3^2$ |
| 25 | 24.99 | 0.0139 | 13.32 | 0.9400 | 0.0023 | 25.83 | 0.9997 | 2.01 | 0.9402 | 5.32 | 0.9968 | 6.98 | 0.9620 |
| 50 | 49.59 | 0.0116 | 24.64 | 0.9715 | 0.0012 | 51.02 | 0.9999 | 0.81 | 0.8241 | 1.13 | 0.8167 | 2.11 | 0.8542 |
| 100 | 88.91 | 0.0103 | 70.91 | 0.8721 | 0.0003 | 91.83 | 0.9935 | 0.03 | 0.9831 | 0.09 | 0.9406 | 1.99 | 0.5740 |

using MMCB. (adsorbent dose, 0.02 g; volume, 20 mL; initial Cr (VI) concentration, 25 mg/L; contact time, 2 h and temperature, 298 ± 2K).

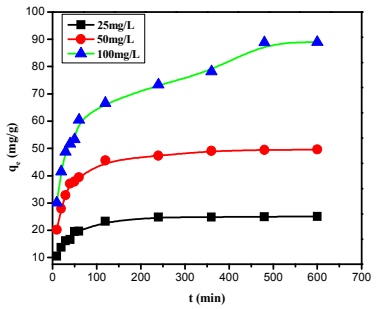


Fig. 4 The effect of contact time of adsorption of Cr(VI) on MMCB. (adsorbent dose, 0.02 g; initial Cr(VI) concentration, 25, 50 and 100 mg/L;volume, 20 mL; pH, 2.0 and temperature, 298± 2K ).

where $q_e$ (mg/g) and $q_t$ (mg/g) are the amounts of Cr(VI) adsorbed at equilibrium time and at any instant of time, $t$, respectively; $k_1$ ($min^{-1}$) and $k_2$ (g ($mg^{-1}$ $min^{-1}$)) are the rate constant of pseudo-first-order and pseudo-second-order model, respectively. The values of $k_1$ and $k_2$ can be determined from the slope of the linear plot of log ($q_e$-$q_t$) *versus* $t$ and $t/q_t$ *versus* $t$, respectively.

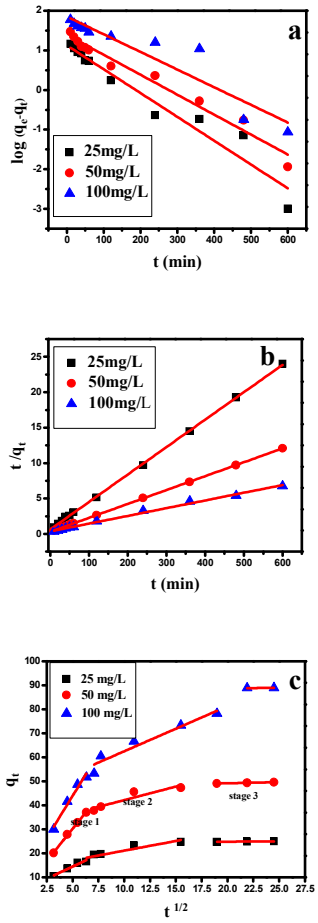


Fig. 5 The adsorption kinetic of pseudo-first-order (a) and pseudo-second-order (b) and the intraparticle diffusion model (c).

The adsorption kinetic models curves were illustrated in Fig. 5a and b, the rate constants and $R^2$ values for the different kinetic models for the adsorption of Cr(VI) were shown in Table 1. It was shown that the kinetic rates of Cr(VI) adsorption with different initial Cr(VI) concentration by MMCB were described less by the pseudo-first-order equation ($R^2$= 0.9400, 0.9715, 0.8721) than by the pseudo-second-order ($R^2$ = 0.9997, 0.9999, 0.9935). Therefore, the adsorption kinetic is not diffusion controlled but chemisorptions.[39]

The adsorption on a porous adsorbent will generally have multi-step process. The intra particle diffusion model proposed by Weber and Morris was also used to model the adsorption data. The plot of $q_t$ *versus* $t^{1/2}$ at different initial Cr(VI) concentrations was depicted in Fig. 5c. As is observed, the plot showed a multi-line nature, indicating that more than one process affected the adsorption. The initial rapid stages were ascribed to the passage of Cr(VI) into the pores of MMCB corresponding to the boundary layer diffusion. The final stage was the residual adsorption process, suggesting that the adsorption could reach ultimate equilibrium. The detailed parameters were illustrated in Table 1.

**Adsorption isotherms**

Adsorption isotherms are usually employed to describe the relationship between the adsorbate concentration in solution and the adsorbate amount adsorbed by the unit mass of adsorbent at a constant temperature at equilibrium. Equilibrium study in adsorption is fundamentally important for the predictive modeling procedures for analyzing and designing an adsorption system. The adsorption isotherms of Cr(VI) on the MMCB were presented in Fig. 6. It is shown that the adsorption capacities increased with the increasing of equilibrium concentrations, and finally approached the maximum adsorption capacities. The adsorption isotherm was studied in 303K, 313K and 323 K, varying the Cr(VI) concentration from 10 to 500 mg/L. Besides, when the initial concentration was lower than 75 mg/L, the residual Cr(VI) in the solution after adsorption by MMCB was negligible. In this study, Langmuir and Freundlich models were adopted to simulate the experimental data, by which the adsorption characteristics between adsorbent and Cr(VI) could have been described.

The Langmuir isotherm model assumed that the adsorption process was monolayer sorption on a homogeneous sorption surface, and all the sorption sites were equal and finite, while the Freundlich isotherm model was an empirical equation for explaining heterogeneous adsorption process.[40] Both the two models were expressed as follows:

Langmuir: $$q_e = \frac{q_m K_L C_e}{1 + K_L C_e}$$

$$R_L = \frac{1}{1 + K_L C_0}$$

Freundlich: $$q_e = K_F C_e^{1/n}$$

where $C_e$ is the equilibrium concentration (mg/L), $C_0$ is the initial concentration (mg/L), $q_e$ is the amount of Cr(VI) adsorbed at equilibrium (mg/g), $q_m$ is the maximum adsorption capacity (mg/g), $R_L$ is the separation factor of the Langmuir. $K_L$ is the Langmuir constant related to the affinity of the binding sites (L/mg), and $K_F$ and $n$ are the Freundlich constants related to the adsorption capacity and intensity, respectively.[41]The adsorption isotherm curves were

Table 2 Parameters of Langmuir and Freundlich isotherm for adsorption of Cr(VI) onto MMCB

| | Langmuir isotherm | | | | Freundlich isotherm | | |
|---|---|---|---|---|---|---|---|
| $T$ (K) | $q_m$ (mg/g) | $K_L$ (L/mg) | $R_L$ | $R^2$ | $K_F$ (mg/g) | $n$ | $R^2$ |
| 303 | 143.20 | 0.1253 | 0.0157-0.4438 | 0.9719 | 45.99 | 4.755 | 0.9009 |
| 313 | 181.29 | 0.1744 | 0.0113-0.3644 | 0.9909 | 57.31 | 4.600 | 0.8889 |
| 323 | 205.97 | 0.1866 | 0.0106-0.3489 | 0.9902 | 60.96 | 4.333 | 0.8834 |

presented in Fig. 7, and the related parameters of the two models were listed in Table 2. It is shown that the correlation coefficient $R^2$ of Langmuir was higher than that of Freundlich, meaning that the adsorption process of Cr(VI) onto MMCB fitted the Langmuir model better than Freundlich model. Moreover, from the equation above, we can see that $0< R_L <1$ obviously, indicating the favourable adsorption of Cr(VI) on MMCB.

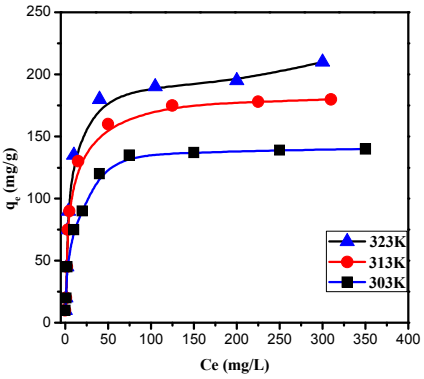


Fig. 6 The effect of temperature on the adsorption of Cr(VI). (adsorbent dose, 0.02 g; volume, 20 mL; pH, 2.0 and contact time, 24 h).

Besides, it is clear from Fig. 6 that the $q_m$ increased with the increase of the temperature. Corresponding to 303K, 313K, and 323K, the values of the $q_m$ were 143.20, 181.29, 205.97 mg/g, respectively.

In addition, the value of $K_L$ increased with temperature. Therefore, the adsorption process of Cr(VI) onto MMCB is endothermic.[36] The comparison with other sodium alginate based materials and carbonaceous materials were listed in Table 3, from which it is clearly demonstrated that MMCB has improved adsorption performance over other similar adsorbents.

**Adsorption thermodynamic**

Thermodynamic consideration of an adsorption process are necessary to deduce whether the process is spontaneous or not, and provide in-depth information about internal energy changes that are associated with the adsorption. Experimental data of Cr(VI) adsorbed on MMCB at equilibrium at different temperatures was used to evaluate the thermodynamic parameters such as enthalpy change ($\Delta H$), Gibbs free energy change ($\Delta G$), and entropy change ($\Delta S$) for the adsorption system by the following equations:

$$\ln K_L = \frac{\Delta S}{R} - \frac{\Delta H}{RT}$$

$$\Delta G = \Delta H - T\Delta S$$

where $K_L$ is the Langmuir constant (L mol$^{-1}$), $R$ is the ideal gas constant (8.314 J mol$^{-1}$ K$^{-1}$) and $T$ is the absolute temperature (K). $\Delta H$ and $\Delta S$ are calculated from the slope and intercept of the linear plot of ln $K_L$ *versus* $1/T$. The $\Delta G$, $\Delta H$, and $\Delta S$ values are listed in Table S2. The negative $\Delta G$ values indicated that the Cr(VI) adsorption processes were thermodynamically feasible and spontaneous under the experimental conditions. The positive value of $\Delta H^0$ (16.00 kJ mol$^{-1}$) for Cr(VI) uptake confirmed the endothermic nature of adsorption, and the positive value of $\Delta S^0$

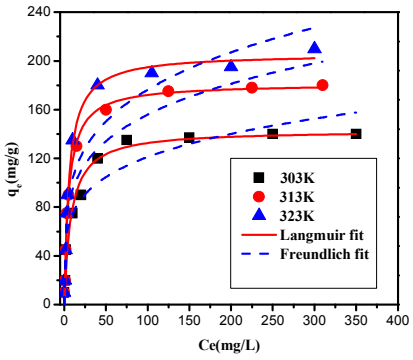


Fig. 7 The adsorption isotherms of Langmuir and Freundlich model.

Table 3 The Cr(VI) adsorption capacity of MMCB compared with other similar materials

| Adsorbent | Adsorption capacity (mg g$^{-1}$) | Reference |
|---|---|---|
| N-ACs | 89 | 13 |
| Bt/Bc/α-$Fe_2O_3$ | 81.7 | 15 |
| CMB | 120 | 16 |
| Oxi-MWCNTS | 85.83 | 32 |
| Fe @ PC | 10 | 38 |
| RHC-mag-CN | 16 | 42 |
| $Fe_3O_4$@Alg-Ce | 14.29 | 43 |
| $Fe_3O_4$/CNT-IL | 55.43 | 44 |

| | | |
|---|---|---|
| MMCB | 143.2 | This work |

(126.16 J $mol^{-1}$ K) suggests an increased randomness occurring at the solid solution interface during the adsorption process.

**Effect of coexisting ions**

Previous investigations revealed that the concentrations of coexistent cations and anions in wastewater containing Cr(VI) generated from electroplating, metal finishing, and leather tanning varied from dozens to hundreds of milligrams per liter (mg $L^{-1}$). As we know, Cr(VI) exist in the form of anions in aqueous phase, and adsorption of Cr(VI) occurs on the adsorbent surface through electrostatic interaction. Thus, the adsorption of Cr(VI) would not be influenced by the cations exist in the solution.[14]

Therefore, the experiments were performed to study the effect of commonly present anions such as $Cl^-$, $NO^{3-}$, $SO_4^{2-}$, and $PO_4^{3-}$ ($C_0$ = 200, 400, 800, 2000 mg/L) on the Cr(VI) uptake. As shown in Fig. 8, all the four anions have the influence of different levels, which is reflected by the following sequence of the Cr(VI) adsorption capacity: $Cl^- > NO^{3-} > SO_4^{2-} > PO_4^{3-}$. The former three anions had less effect on the removal of Cr(VI), and the $PO_4^{3-}$ concentration less than 2000 mg/L was slightly effected. However, when the $PO_4^{3-}$ concentration is 2000 mg/L, the Cr(VI) adsorption capacity decreased from 47.75 to 6.86 mg/g. This phenomenon is possibly due to the competition mechanism. As for $Cl^-$ and $NO^{3-}$, which are monovalent anions, they may slightly compete with the chromium anion for the positive charge adsorption sites on the MMCB surface. By contrast, the $SO_4^{2-}$ and the $PO_4^{3-}$ are multivalent anions, which could significantly compete with $Cr_2O_7^{2-}$, $HCrO_4^-$, and $CrO_4^{2-}$ for more available sorption sites of the MMCB.[36] When the $PO_4^{3-}$ concentration reached 2000 mg/L, almost all the sorption sites were surrounded by $PO_4^{3-}$, the repulse interaction between two anions would be strengthened, the chromium anions could not reach the MMCB surface; hence, the Cr(VI) adsorption would be inhabited dramatically. The study of coexisting anions on Cr(VI) uptake demonstrated that electrostatic force is one of possible adsorption mechanism for the removal of Cr(VI) by MMCB.

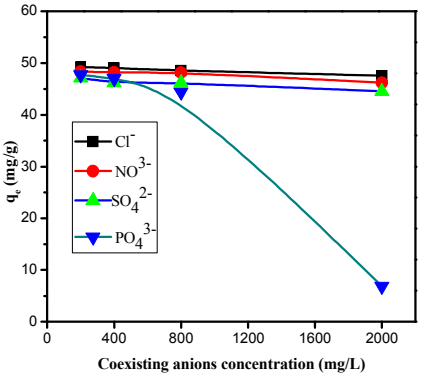


Fig. 8 The effect of coexisting ions on the adsorption of Cr(VI). (adsorbent dose, 0.02 g; volume, 20 mL; Cr (VI) concentration, 50 mg/L; contact time, 4 h and temperature, 298 ± 2K).

**Desorption and reusability study**

To make the adsorption media cost effectively for Cr(VI) removal from industrial wastewater, it is necessary that the MMCB should be reused for repeated cycles. Desorption experiments were performed as follows: 0.02 g MMCB was added to 20 mL of 50 mg/L Cr(VI) solutions with the same conditions of the adsorption experiments. When the adsorption reached equilibrium, placing an external magnetic field under the conical flask, the Cr-loaded MMCB would be separated fast and easily. Then, the Cr-loaded MMCB was left in the flask and rinsed with ultrapure water to remove residual solution trapped among the MMCB. Subsequently, 20 mL, 2M NaOH solution added into the flask as eluent. Adsorbent was rinsed with 1M HCl and deionized water till the supertant pH was neutral before the second adsorption cycle. As can be observed in Fig. 9, the removal efficiency of Cr(VI) on MMCB was still high in the fifth regeneration cycle, it could still reached more than 80%. The decrease of removal efficiency can be ascribed to the loss of partial reduction property of MMCB and the inevitable mass loss during the repeated adsorption process. Therefore, the above experimental results demonstrated that this new adsorbent could be easily regenerated and reused by simple treatment; it has the potentiality for treatment of wastewater contaminated by highly toxic Cr(VI).

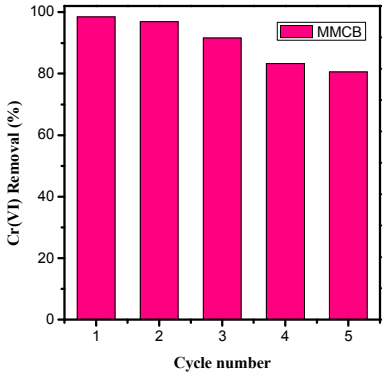


Fig. 9 The reusability of MMCB on the adsorption of Cr(VI). (adsorbent dose, 0.02 g;Cr (VI) concentration, 50 mg/L; pH, 2.0; contact time, 4 h and temperature, 298 ± 2K).

**The stability testing of MMCB**

Since the adsorbent was of monolithic material, it could not be observed the obvious damage in the experiment process. To this end, the stability of MMCB was evaluated through determining the concentrations of the dissolved iron ions in the solution during the five consecutive cycles. The results showed that the concentrations of the iron ions in the solution were at a minimal level (<0.1 mg $L^{-1}$) during all the cycles, which was below the maximum acceptable iron concentration in drinking water, as 0.3 mg $L^{-1}$, set by the WHO. Thus, it can be indicated that MMCB exhibited good stability and can be applied as a promising adsorbent to remove Cr(VI) from water with negligible loss of its magnetic properties.

**Adsorption mechanism**

The above analysis results have shown that the large surface area of MMCB was beneficial for the adsorption for the removal of Cr(VI), owing to the large amounts of accessible adsorption sites. To gain further insight into the uptake mechanism of Cr(VI), the FTIR technology was used to analyze the surface change of MMCB before and after adsorption. As shown in Fig. S7, distinct changes can be observed after adsorption of Cr(VI). The –OH shifted from 3421 to 3427 $cm^{-1}$, this might be ascribed to the electrostatic interaction

between the protonated oxygen-contained groups and chromium ions.[14] Also, the intensity of –C-H at 1378 $cm^{-1}$ changed slightly after adsorption of Cr(VI), because of the –C-H function groups had relative reducing ability under weak acidic condition; therefore it may also participate the removal of Cr(VI).[38]

Moreover, XPS spectra of MMCB surfaces before and after Cr(VI) adsorption were studied to elaborate the uptake process of Cr(VI). The XPS total survey spectrum of MMCB of comparison with MMCB-Cr was shown in Fig. 10A. It was obvious that two peaks at 577 and 587 eV appears and it ascribed to the Cr $2p_{3/2}$ and Cr $2p_{1/2}$.[32] This indicated that the Cr(VI) was tackled by MMCB successfully. The presence of the elements C, O and Fe with high contents in the MMCB was evidenced by the photoelectron lines of wide-scan spectrum with binding energies at 285, 532 and 711 eV, attributed to C 1s, O 1s and Fe 2p, respectively. The high resolution of Cr 2p spectrum was depicted in Fig. 10B. The Cr $2p_{1/2}$ and Cr $2p_{3/2}$ could be further fitted into two peaks, respectively. The ones at 587.86 and 586.68 eV were assigned to the Cr $2p_{1/2}$ of Cr(VI) and Cr(III), while those at 577.88 and 576.79 eV to the Cr $2p_{3/2}$ of Cr(VI) and Cr(III), indicating that Cr(VI) and Cr(III) coexisted on the pore surface of MMCB. Fig. 10C and D displayed the C 1s spectra of MMCB before and after Cr(VI) adsorption. In Fig. 10C, the peaks at 285.3, 284.8, 284.4 and 283.9 eV were ascribed to C-OH, C = C, C-H and C-C, respectively. After adsorption of Cr (VI), it was depicted in Fig. 10D, the peak of C 1s became broader and could be further fitted into four peaks. The peaks located in 285.96, 284.97, 284.47 and 283.99 eV were the characteristics of C-OH, C = C, C-H and C-C, respectively.[31] By careful comparison, it was found that the intensity of C-OH became weaker after adsorption, which can be explained by the electrostatic interaction or redox reaction.

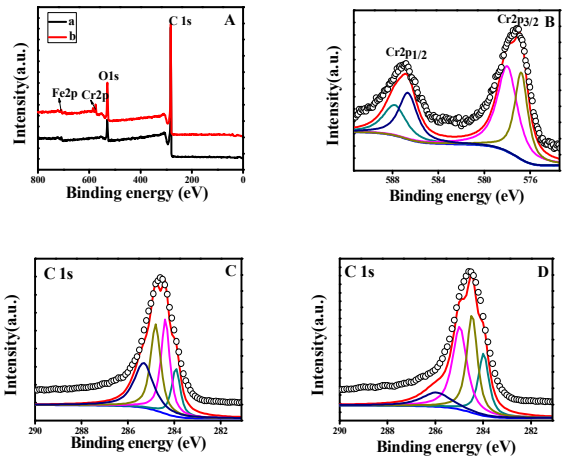


Fig. 10 The XPS spectra of the survey of MMCB (a)and MMCB-Cr (b) (A), the high resolution of Cr 2p spectrum (B), and the C 1s of MMCB (C) and MMCB-Cr (D).

Additionally, to our knowledge, C-H and C-OH groups were the strongest reducing groups on the carbon surface. Therefore it could be reasonably speculated that the surface reducing groups, C-H and C-OH groups, could reduce the adsorbed Cr(VI) to Cr(III), and in turn they were oxidized. However, no COOH was found on the carbon surface, which was consistent with the FTIR spectrum and could be interpreted by the following equations:[38]

$$\text{-C-H} + \text{Cr(VI)} + H_2O \rightarrow \text{-C-OH} + \text{Cr(III)} + H^+$$

$$\text{-C-OH} + \text{Cr(VI)} + H_2O \rightarrow \text{–C=O} + \text{Cr(III)} + H^+$$

$$\text{-C=O} + \text{Cr(VI)} + H_2O \rightarrow \text{–COOH} + \text{Cr(III)} + H^+$$

$$\text{-C-COOH} + \text{Cr(VI)} + H_2O \rightarrow \text{–C-H} + \text{Cr(III)} + H^+ + CO_2\uparrow$$

The $H^+$ which produced in the redox reaction can be explained the equilibrium pH was lower than initial solution pH.

On the basis of the above analysis, the main reaction proceeding between Cr(VI) and the MMCB is proposed in Scheme 2. First, the –OH groups on the adsorbent were protonated under the acidic conditions, and thus the surface complexation occurred between protonated functional groups and aqueous Cr(VI) oxyanions *via* electrostatic attraction. Then, because of its strong oxidation ability, the adsorbed Cr(VI) can react with the reducing groups, a few Cr(VI) oxyanions were reduced to Cr(III) cations. Finally, the majority of Cr(III) deposited on the carbon surface and extremely small amount of residual Cr(III) released into solution again.

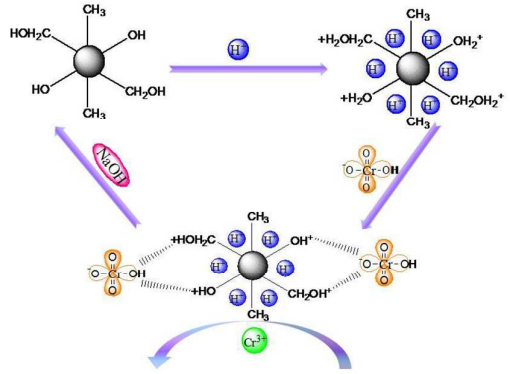


Scheme 2 The possible mechanism of Cr(VI) adsorption on MMCB.

## Conclusion

In summary, a new type of magnetic monolithic material was successfully fabricated and employed as an adsorbent for Cr(VI) removal. Batch adsorption experiment showed that the adsorption of Cr(VI) was dependent on solution pH, contact time, initial concentration, temperature and coexisting anions. The adsorption kinetics followed pseudo-second-order kinetic equation, and the equilibrium data could be fitted by the Langmuir isotherm. Thermodynamic studies indicated the endothermic and spontaneous nature of the adsorption process. The reusability and stability test showed that the material can be reused easily and would kept integrity under the experiment condition. The mechanism investigation revealed that Cr(VI) adsorption on MMCB involved electrostatic interaction and redox reaction. Owing to its integrated advantages of monolithic, magnetic and stable property, this new material can be a promising candidate for the treatment of Cr(VI)-containing wastewater efficiently. In conclusion, this method of synthesizing monolithic magnetic materials offered new opportunities in finding effective, convenient and economic treatment to removal Cr(VI) and other heavy metals contaminant from wastewater.

## Acknowledgments

Financial support from the National Natural Science Foundation of China (21446001), the Program for Liaoning Innovative Research Team in University (LT2013012) and the Program for Liaoning Excellent Talents in University (LJQ2014056) is highly appreciated.

**Notes and references**

1 N. X.Wang, X. Y. Zhang, J.Wu, L. Xiao, Y. Yin, A. J.Miao, R. Ji and L. Y. Yang, Water Res., 2012, 46, 369–377.
2 Y. Y. Sun, Q. Y. Yue, Y. P. Mao, B. Y. Gao, Y. Gao and L. H. Huang, *J. Hazard. Mater.*, 2014, **265**, 191–200.
3 J.H. Wang, C.P. Huang, C.H. Weng, *Water Sci. Technol.*, 1997, **35**, 55–62.
4 C. Gan, Y.G. Liu, X.F. Tan, *RSC Adv.*, 2015, **5**, 35107-35115.
5 Geneva, Health criteria and other supporting information, Guidelines for Drinking-Water Quality, ed. WHO, World Health Organization, 1996, **2**, 1–13.
6 R. C. Thomson , M. K. Miller, *Acta. Mater.*, 1998, **46**, 2203–2213.
7 S. Mustafa, K. H. Shah, A. Naeem, M. Waseem and M. Tahir, *J. Hazard. Mater.*, 2008, **160,**1–5.
8 C. A. Kozlowski and W. Walkowiak, *Water Res.*, 2002, **36**, 4870–4876.
9 E. Salazar, M. I. Oritiz, A. M. Urtiaga and J. A. Irabien, *Ind. Eng.Chem.Res.*, 1992, **31**, 1516–1522.
10 J. Dui , G. Zhu , and S. Zhou, *ACS Appl. Mater. Interfaces.*, 2013, **5 (2)**, 10081–10089.
11 Y. Chen, G. Gu, *Bioresour. Technol.*, 2005, **96**, 1713–1721.
12 X. Jing, Y. Cao, X. Zhang, D. Wang, X. Wu, H. Xu, *Desalination.*, 2011, **269**, 120–127.
13 J. Zhang, T. Shang, X. Jin, J. Gao and Q. Zhao, *RSC Adv.*, 2015, **5**, 784–790.
14 L. Deng, Z. Shi and X. Peng, *RSC Adv.*, 2015, **5**, 49791–49801.
15 Z. Ruan, J. Wu, J. Huang, Z. Lin, Y. Li, Y. Liu, Pi. Cao, Y. Fang, J. Xie and G. Jiang, *J. Mater. Chem. A*., 2015, **3**, 4595–4603.
16 M. Zhang, Y. Liu, T. Li, W. Xu, B. Zheng, X.i Tan, H. Wang, Y. Guo, F. Guo and S. Wang, *RSC Adv.*, 2015, **5**, 46955–46964.
17 X. H. Zhao, Q. Li, X. M. Ma, Z. Xiong, F. Y. Quan and Y. Z. Xia, *RSC Adv.*, 2015, **5**, 49534–49540.
18 V. Rocher, J. Siaugue, V. Cabuil, A. Bee, *Water Res.*, 2008, **42**, 1290–1298.
19 A. Mohammadi, H. Daemi, M. Barikani, *Int. J. Biol. Macromol.*, 2014, **69**, 447–455.
20 S. K. Nadavala, K. Swayampakula, V. M. Boddu, K. Abburi, *J. Hazard. Mater.*, 2009, **162**, 482–489.
21 P. Sikorski, F. Mo, G. Skjak-Braek and B. T. Stokke, *Biomacromolecules.*, 2007, **8**, 2098–2103.
22 L. Li, Y. Fang, R. Vreeker and I. Appelqvist, *Biomacromolecules.*, 2007, **8**, 464–468.
23 Y. Chen, S.R. Zhai, N. Liu, Y. Song, Q.D. An, and X.W. Song, *Bioresour. Technol.*, 2013, **144**, 401-409.
24 Y. Zhao, S.R. Zhai, B. Zhai, and Q.D. An, *J. Sol-Gel Sci. Technol.*, 2012, **62**, 177-185.
25 J.M. Zhang, S.R. Zhai, S. Li, Z.Y. Xiao, Y. Song, Q.D. An, and G. Tian, *Chem. Eng. J.*, 2013, **215-216**, 461-471.
26 S.X. Huang, Z.Y. Xiao, S.R. Zhai, B. Zhai, F. Zhang, Q.D. An, *RSC Adv.*, 2014, **4(105)**, 60460-60466.
27 W.J. Qiao, S.R. Zhai, F. Zhang, Z.Y. Xiao, Q.D. An, X.W. Song, *J. Sol-Gel Sci. Technol.*, 2014, **70**, 451-463.
28 P. Guo, S.R. Zhai, Z.Y. Xiao, Q.D. An, *J. Colloid Interface Sci.*, 2015, **446**, 155-162.
29 H. Guo**,** S.F. Zhang**,** Z.N. Kou**,** S.R. Zhai**,** W. Ma**,** Y. Yang**,** *Carbohyd. Polym.*, 2015, **115**, 177-185.
30 Z. Jiang, Y. Liu, G. Zeng, W. Xu, B. Zheng, X. Tan and S. Wang, *RSC Adv.*, 2015, **5** , 25389–25397.
31 X. Zhang, Y. Li, G. Li and C. Hu, *RSC Adv.*, 2015, **5**, 4984–4992.
32 A. S. K. Kumar, S. Jiang and W. Tseng, *J. Mater. Chem. A*, 2015, **3**, 7044–7057.
33 S. Yang, L. Chen ,L. Mu , P. Ma, *J. Colloid Interface Sci.*, 2014, **430**, 337–344.
34 J. Ma, L. Zhou , W. Dan, H. Zhang, Y. Shao, C. Bao, L. Jing, *J. Colloid Interface Sci.*, 2015, **446**,298–306.
35 A. Chen, Y. Yu, Y. Zhang, T. Xing, Y. Wang, Y. Zhang, J. Zhang, *J. Hazard. Mater.*, 2014, **279**, 280–288.
36 G. Yang, L. Tang, Y. Cai, G. Zeng, P. Guo, G. Chen, Y. Zhou, J. Tang, J. Chen and W. Xiong, *RSC Adv.*, 2014, **4**, 58362–58371.
37 B. Qiu, C. Xu, Z. Guo, and S. Wei, *ACS Sustainable Chem. Eng.*, 2014, **2**, 2070−2080.
38 L. Zhuang , Q. Li, J. Chen , B. Ma , S. Chen, *Chem. Eng. J.*, 2014, **253**, 24-33.
39 G. X. Yang and H. Jiang**,** *Water Res.*, 2014, **48**, 396–405.
40 Q. Cao, F. Huang, Z. Zhuang and Z. Lin, *Nanoscale*, 2012, **4**, 2423-2430.
41 A. Kara, E. Demirbel, N. Tekin, B. Osman, N. Besiril, *J. Hazard. Mater.*, 2015, **286**, 612-623.
42 Y. Li, S. Zhu , Q. Liu , Z. Chen , J. Gu ,C. Zhu , T. Lu , D. Zhang , J. Ma, *Water Res.*, 2013, **47**, 4188-4197.
43 V. Gopalakannana, N. Viswanathan, *Int. J. Biol. Macromol.*, 2015, **72**, 862–867.
44 C. Wu,J. Fan,J. Jiang and J. Wang, *RSC Adv.*, 2015, **5**, 47165–47173.
45 M. S. Moorthy, D. Seo, H. Song, S. S. Park and C. S. Ha, *J. Mater. Chem. A*, 2013, **1**, 12485-12496.
46 D. Li, D. Yang, X. Zhu, D. Jing, Y. Xia, Q. Ji, R. Cai, H. Li and Y. Che, *J. Mater. Chem. A*, 2014, **2**, 18761-18766.

NJC

ARTICLE

## Graphical Abstracts

# Monolithic magnetic carbonaceous beads for efficient Cr(VI) removal from water

Zhi-Min Lei, Qing-Da An*, Yuan Fan, Jia-Liang Lv, Ce Gao, Shang-Ru Zhai*, Zuo-Yi Xiao

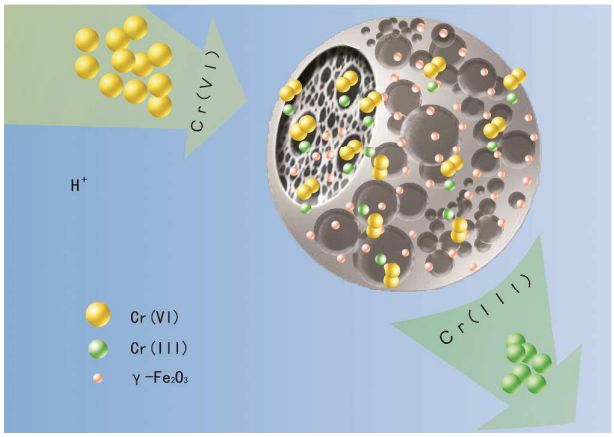


Alginate-derived magnetic monolithic carbonaceous beads, aiming for efficient Cr(VI) removal, easy recovery and expectable reusability, was firstly synthesized.